Journal of Geophysical Research: Solid Earth

Supporting Information for

Major mineral fraction and physical properties of carbonated peridotite (listvenite) from ICDP Oman Drilling Project Hole BT1B inferred from the X-ray CT core images

Keishi Okazaki[1*], Katsuyoshi Michibayashi[2], Kohei Hatakeyama[3], Natsue Abe[4], Kevin T.M. Johnson[3], Peter B. Kelemen[4], and the Oman Drilling Project Phase I Science Party

[1]Kochi Institute for Core Sample Research, Japan Agency for Marine-Earth Science and Technology (X-star, JAMSTEC), Kochi 783-8502, Japan

[2]Department of Earth and Planetary Sciences, Graduate School of Environmental Studies, Nagoya University, Aichi 464-8602, Japan

[3]Department of Earth and Planetary Systems Science, Hiroshima University, Hiroshima 739-8526, Japan

[4]Mantle Drilling Promotion Office, Japan Agency for Marine-Earth Science and Technology (MarE3, JAMSTEC), Kanagawa 236-0001, Japan

[5]Department of Earth Sciences, University of Hawai'i at Mānoa, Hawaii 96822, USA

[6]Lamont Doherty Earth Observatory, Columbia University, New York 10964, USA

*Corresponding author: Keishi Okazaki (JAMSTEC, Japan)

E-mail: okazakik@jamstec.go.jp; Tel: +81-88-878-2244; Fax: +81-88-878-21924

Contents of this file

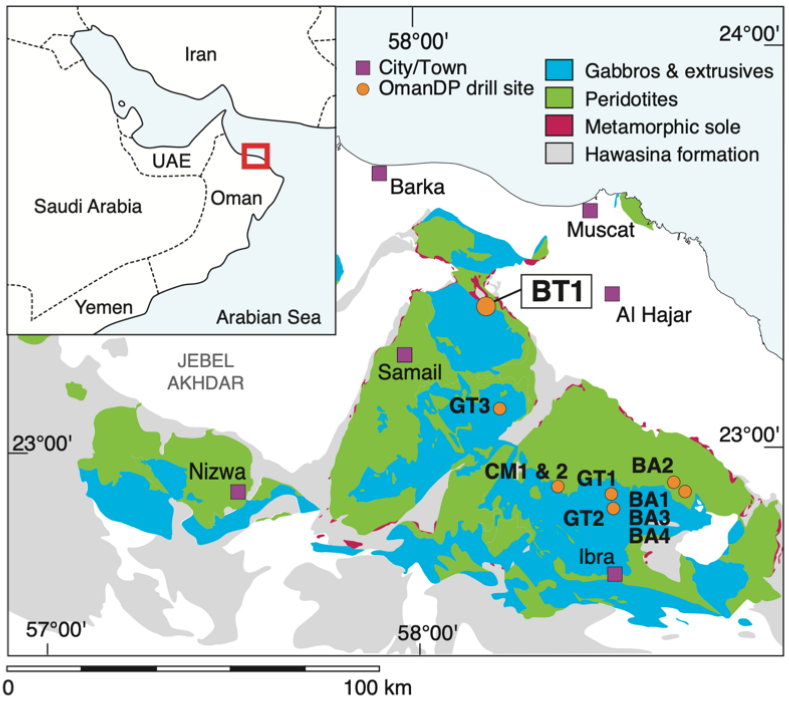

Figure S1. Geological map of the southeastern massif of the Samail ophiolite (after Nicolas et al., 2000) showing the drill site locations of the ICDP Oman Drilling Projects.

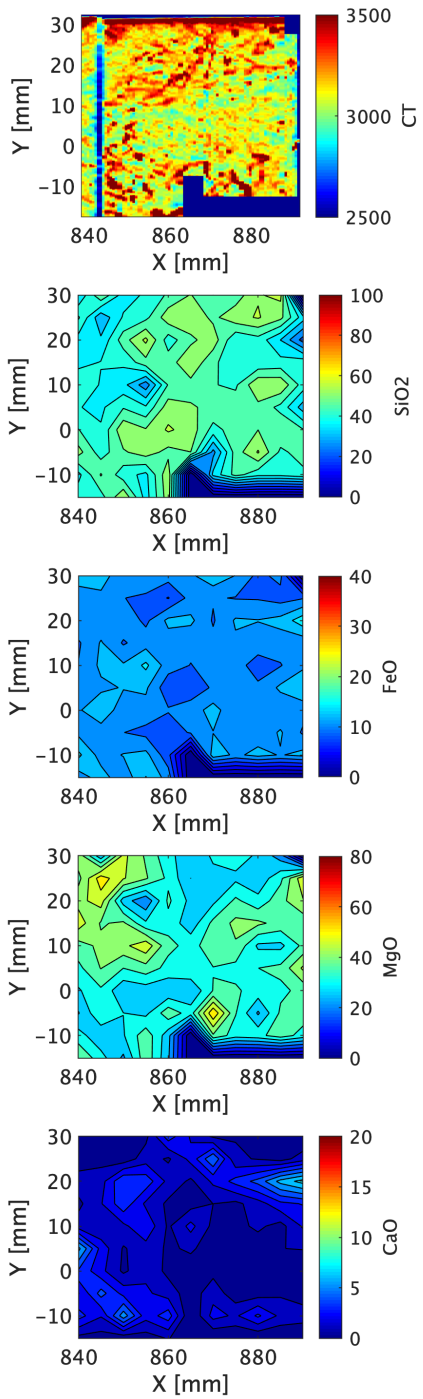

Figure S2. Comparison among (a) the XCT image, (b) SiO2, (c) FeO, (d) MgO and (e) CaO chemical mappings from the XRF scanner from the core section 12Z-1 84–89 cm.

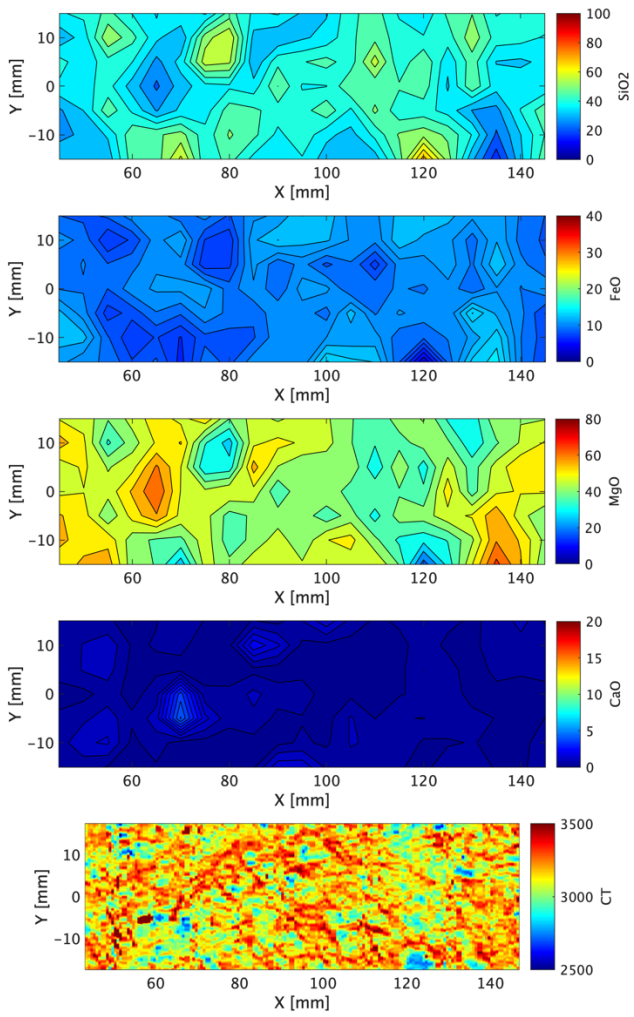

Figure S3. Comparison among (a) SiO2, (b) FeO, (c) MgO and (d) CaO, and (e) the XCT image, mappings from the XRF scanner and XCT from the core section 13Z-4 5–15 cm.

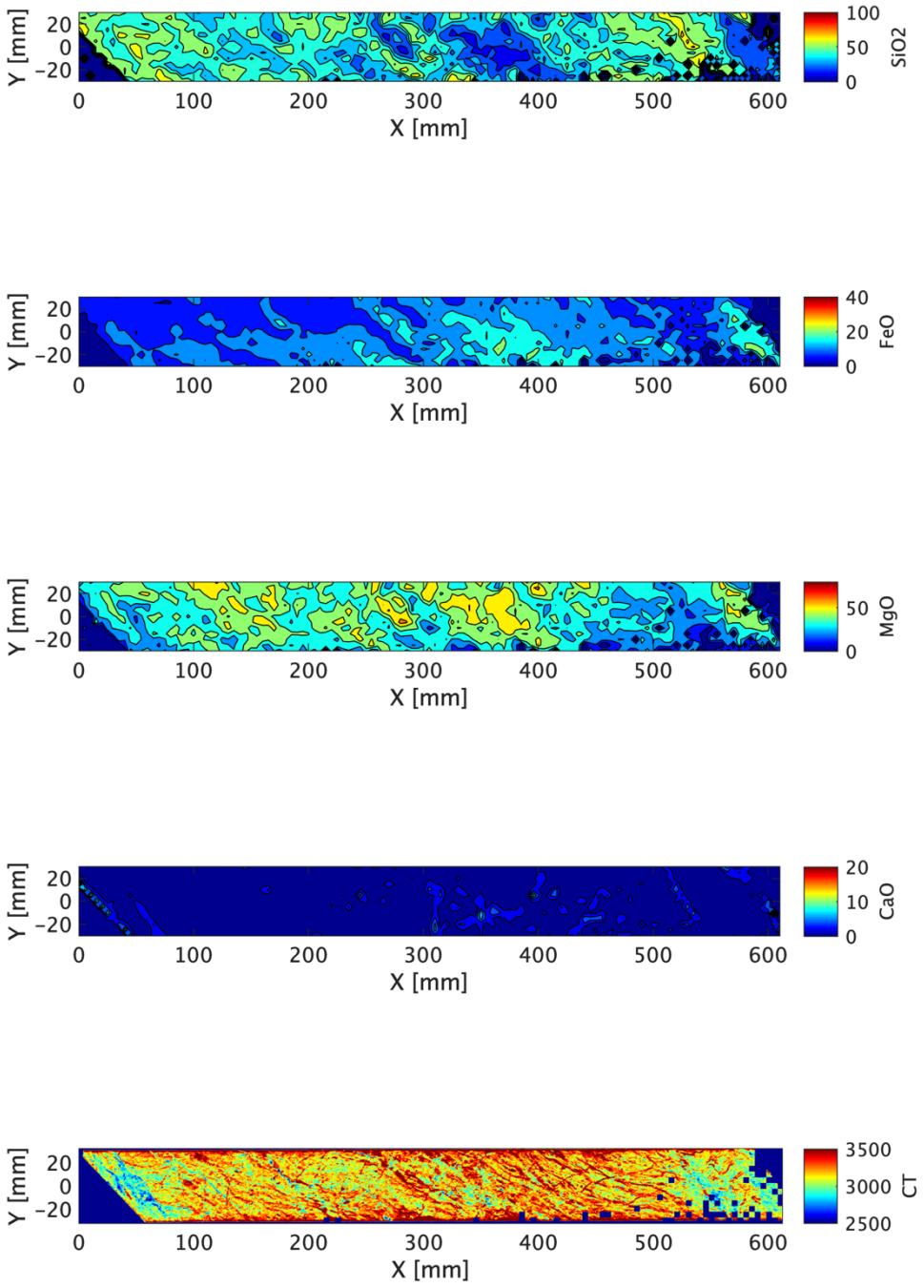

Figure S4. Comparison among (a) SiO2, (b) FeO, (c) MgO and (d) CaO, and (e) the XCT image, mappings from the XRF scanner and XCT from the core section 14Z-2 0–61 cm.

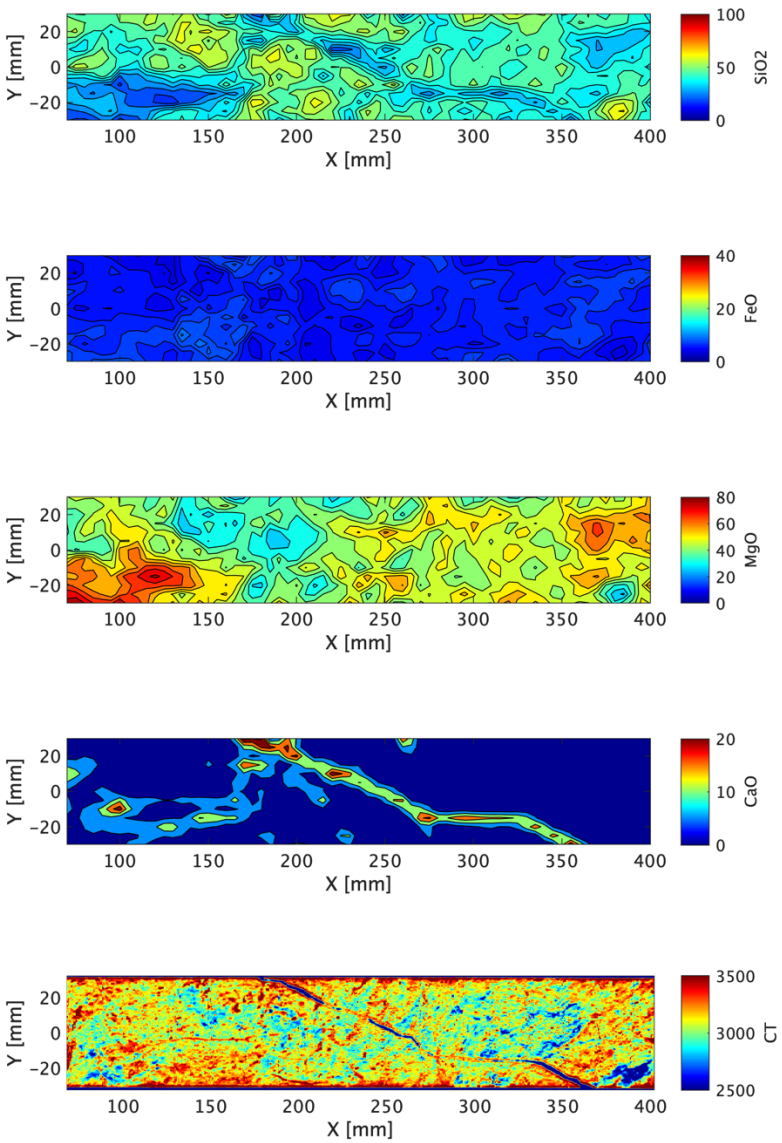

Figure S5. Comparison among (a) SiO2, (b) FeO, (c) MgO and (d) CaO, and (e) the XCT image, mappings from the XRF scanner and XCT from the core section 16Z3 7–40 cm.

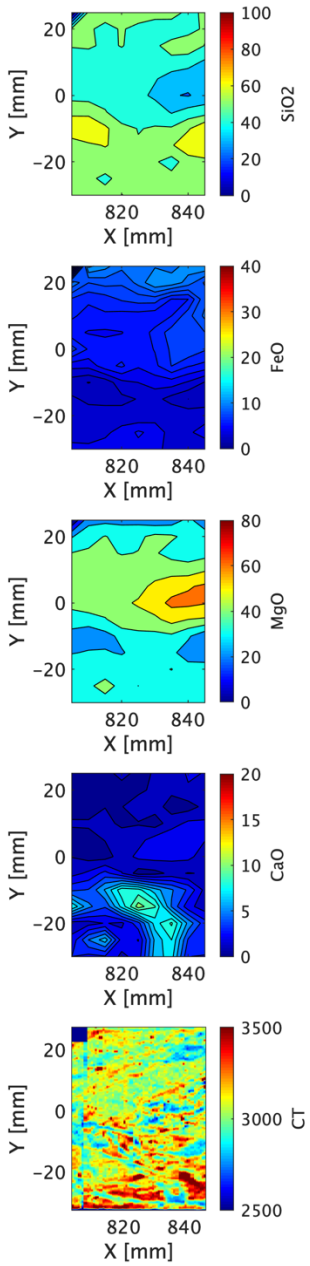

Figure S6. Comparison among (a) SiO2, (b) FeO, (c) MgO and (d) CaO, and (e) the XCT image, mappings from the XRF scanner and XCT from the core section 20Z-1 78–83 cm.

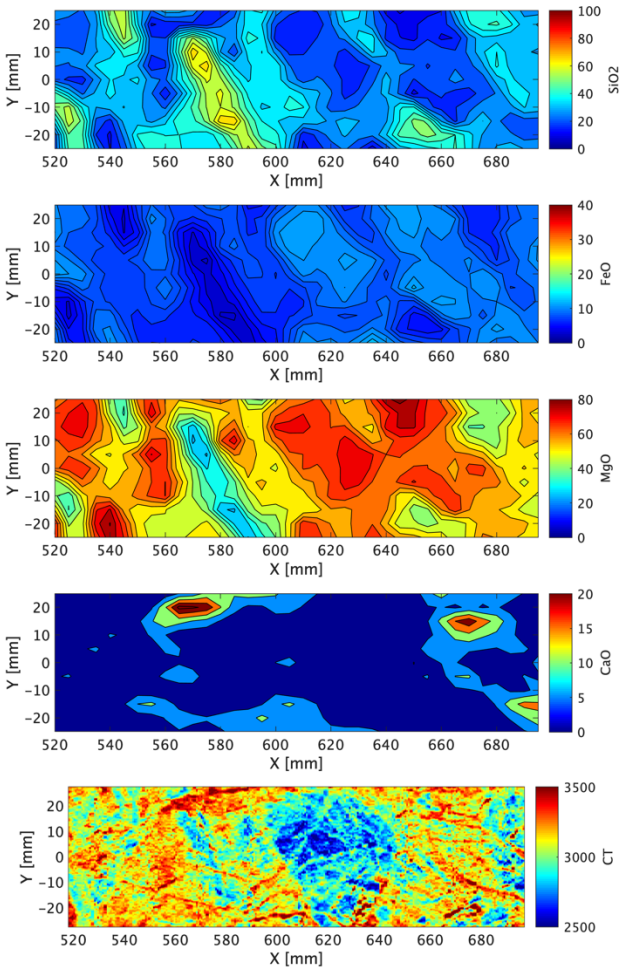

Figure S7. Comparison among (a) SiO2, (b) FeO, (c) MgO and (d) CaO, and (e) the XCT image, mappings from the XRF scanner and XCT from the core section 28Z-1 49–71 cm.

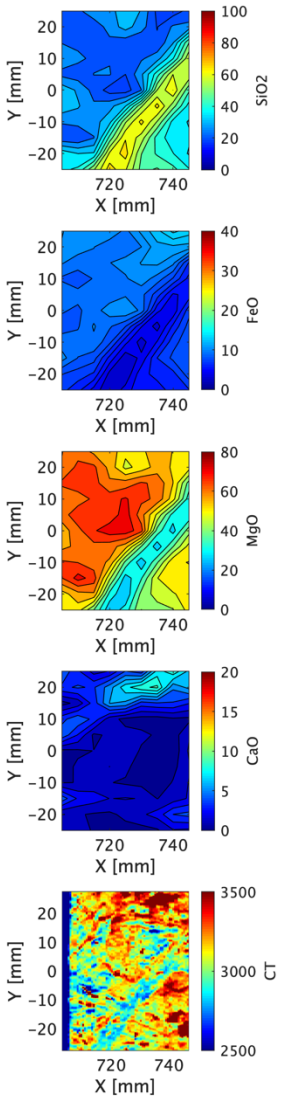

Figure S8. Comparison among (a) SiO2, (b) FeO, (c) MgO and (d) CaO, and (e) the XCT image, mappings from the XRF scanner and XCT from the core section 28Z-1 69–74 cm.

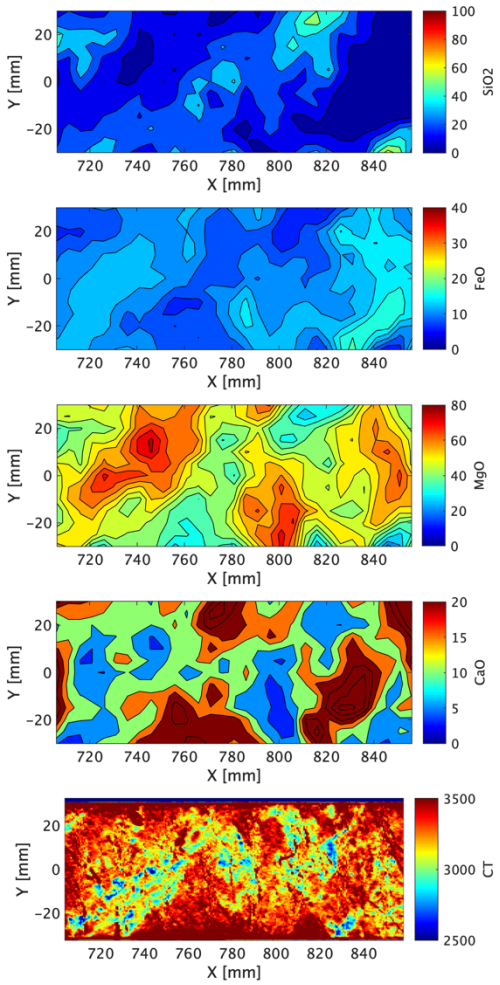

Figure S9. Comparison among (a) SiO2, (b) FeO, (c) MgO and (d) CaO, and (e) the XCT image, mappings from the XRF scanner and XCT from the core section 32Z-2 70–85 cm.

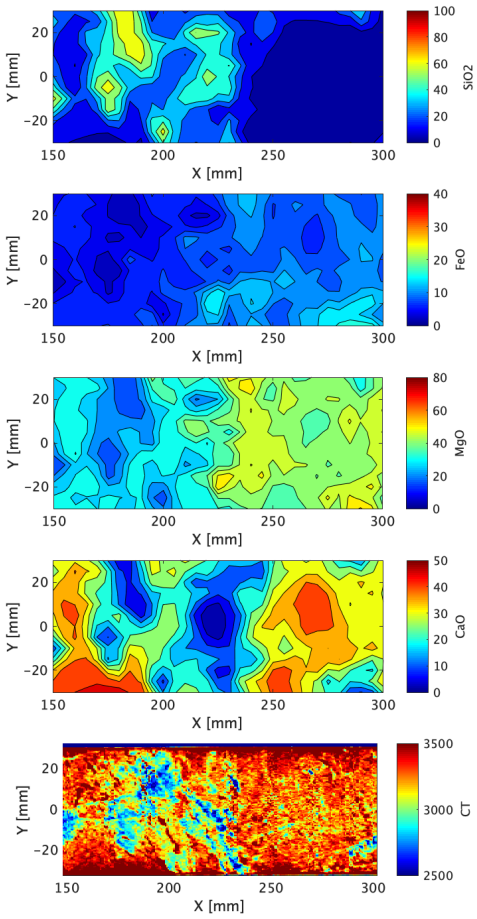

Figure S10. Comparison among (a) SiO2, (b) FeO, (c) MgO and (d) CaO, and (e) the XCT image, mappings from the XRF scanner and XCT from the core section 32Z-3 15–30 cm.

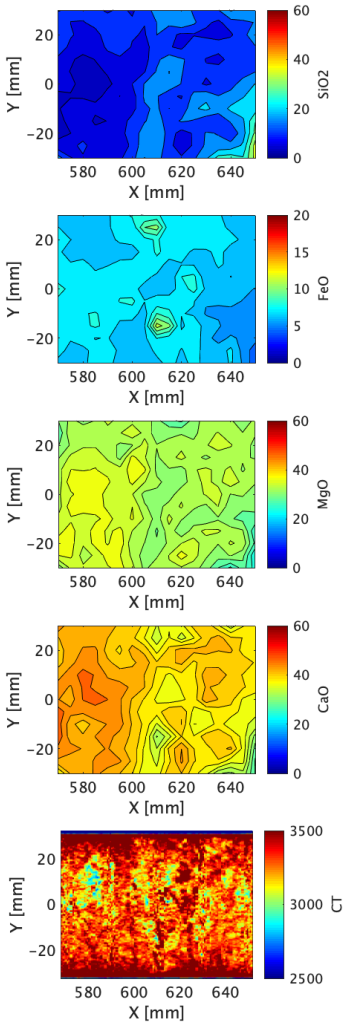

Figure S11. Comparison among (a) SiO2, (b) FeO, (c) MgO and (d) CaO, and (e) the XCT image, mappings from the XRF scanner and XCT from the core section 32Z-3 57–65 cm.

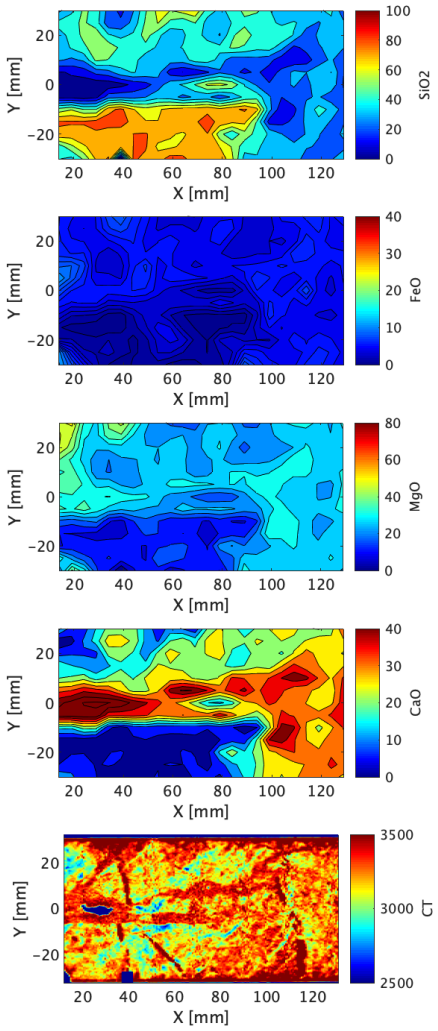

Figure S12. Comparison among (a) SiO2, (b) FeO, (c) MgO and (d) CaO, and (e) the XCT image, mappings from the XRF scanner and XCT from the core section 32Z-4 0–12 cm.

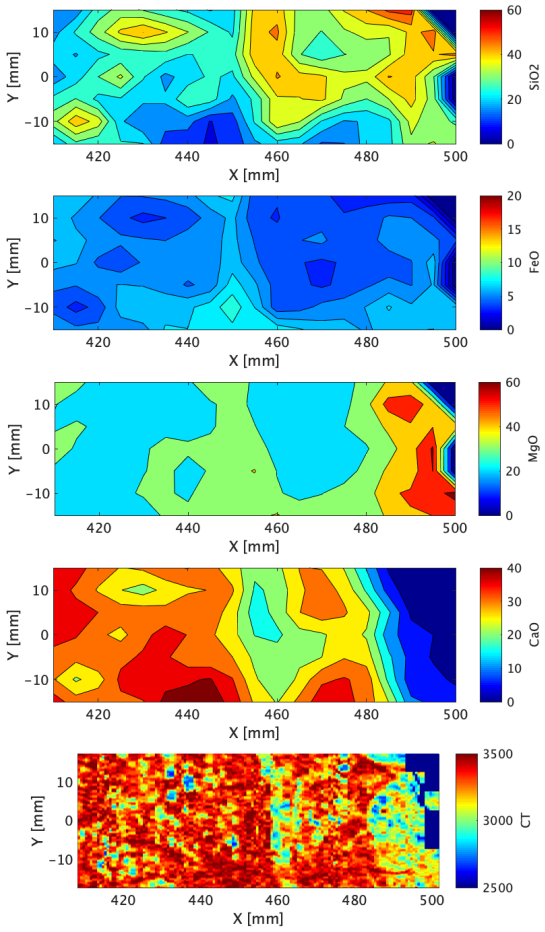

Figure S13. Comparison among (a) SiO2, (b) FeO, (c) MgO and (d) CaO, and (e) the XCT image, mappings from the XRF scanner and XCT from the core section 47Z-4 41–50 cm.

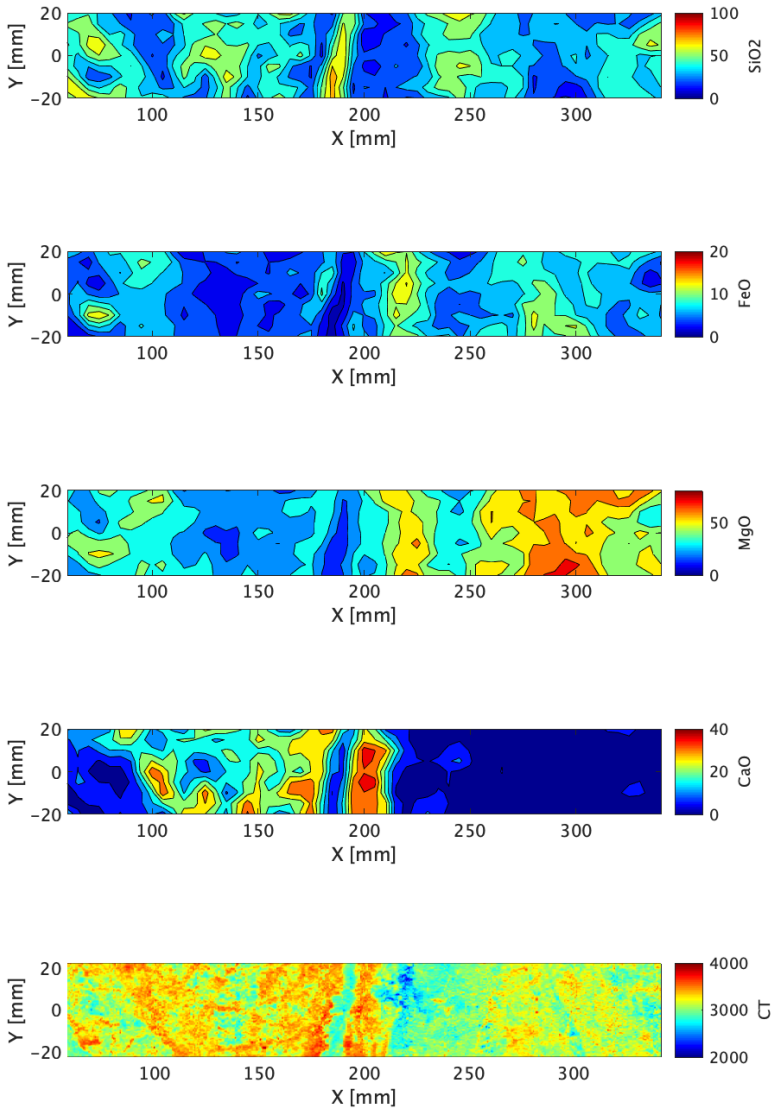

Figure S14. Comparison among (a) SiO2, (b) FeO, (c) MgO and (d) CaO, and (e) the XCT image, mappings from the XRF scanner and XCT from the core section 49Z-2 6–34 cm.

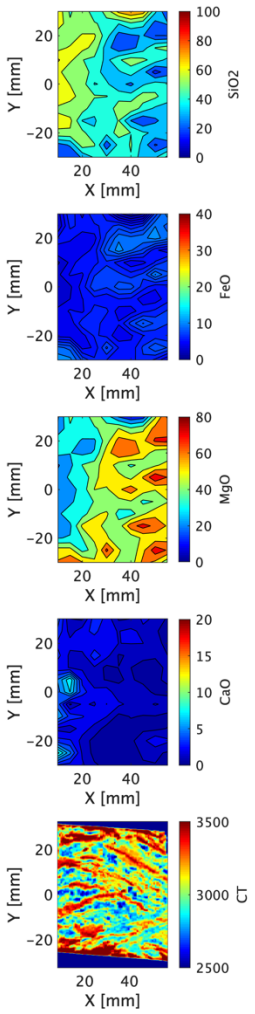

Figure S15. Comparison among (a) SiO2, (b) FeO, (c) MgO and (d) CaO, and (e) the XCT image, mappings from the XRF scanner and XCT from the core section 52Z-2 1–4 cm.

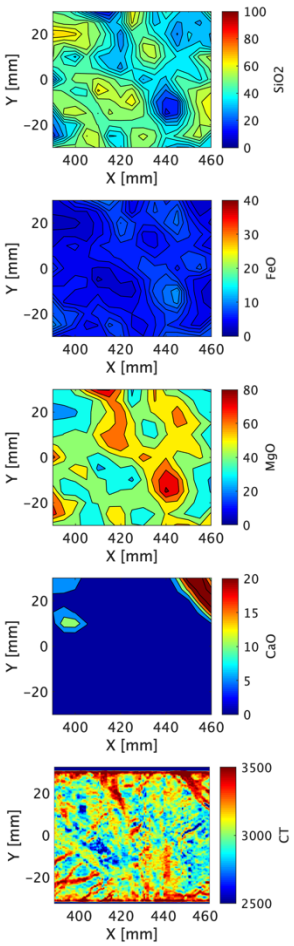

Figure S16. Comparison among (a) SiO2, (b) FeO, (c) MgO and (d) CaO, and (e) the XCT image, mappings from the XRF scanner and XCT from the core section 52Z-2 39–46 cm.

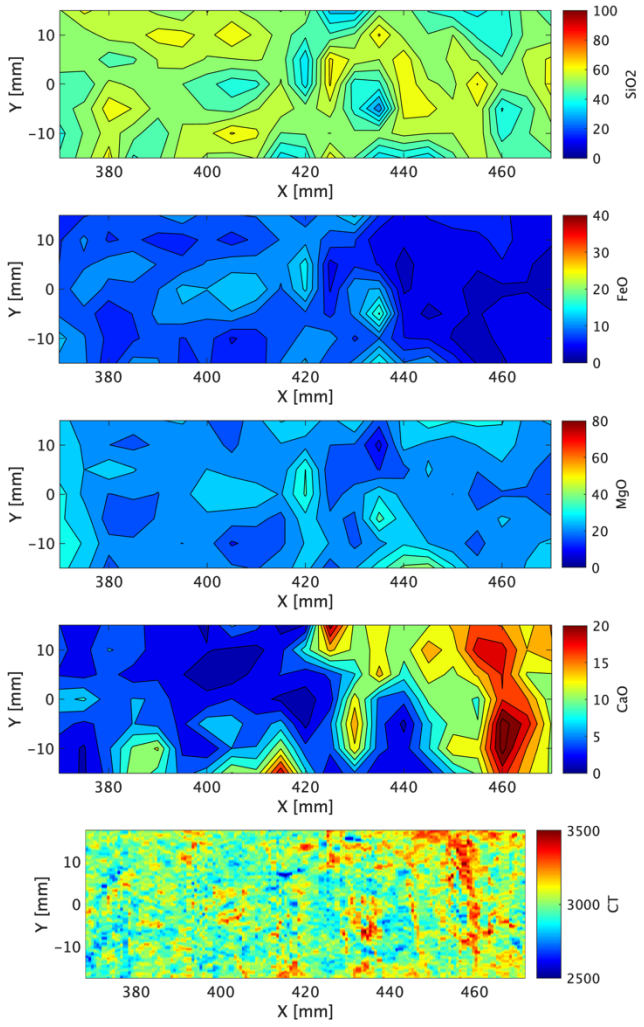

Figure S17. Comparison among (a) SiO2, (b) FeO, (c) MgO and (d) CaO, and (e) the XCT image, mappings from the XRF scanner and XCT from the core section 53Z-4 37–47 cm.

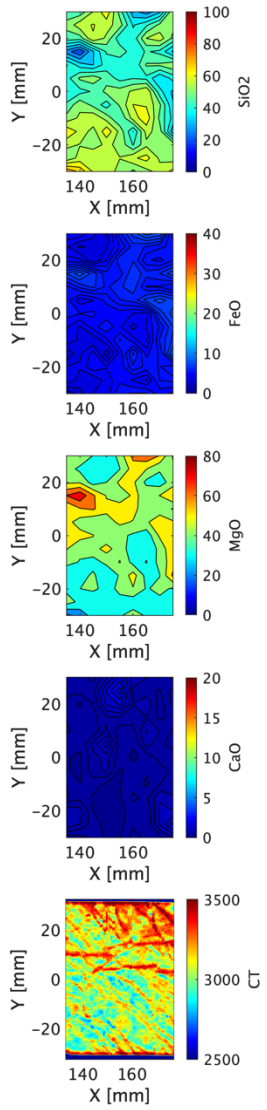

Figure S18. Comparison among (a) SiO2, (b) FeO, (c) MgO and (d) CaO, and (e) the XCT image, mappings from the XRF scanner and XCT from the core section 60Z-1 12–17 cm.

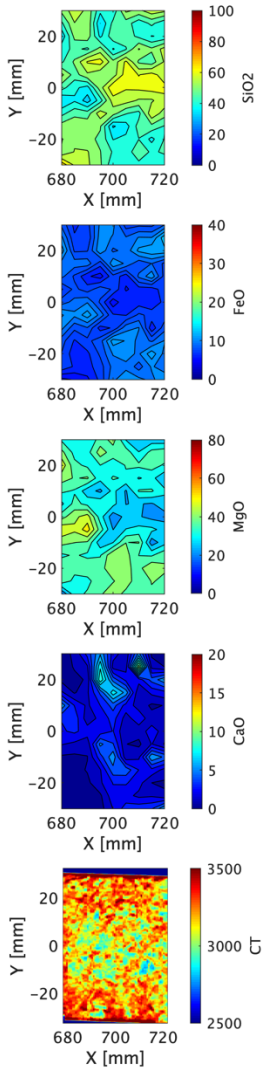

Figure S19. Comparison among (a) SiO2, (b) FeO, (c) MgO and (d) CaO, and (e) the XCT image, mappings from the XRF scanner and XCT from the core section 66Z-3 66–71 cm.

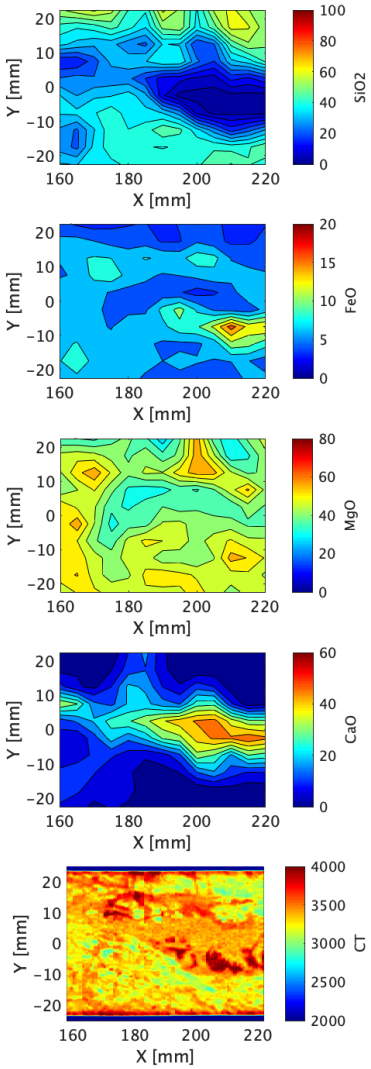

Figure S20. Comparison among (a) SiO2, (b) FeO, (c) MgO and (d) CaO, and (e) the XCT image, mappings from the XRF scanner and XCT from the core section 73Z-2 16–22 cm.

Table S1. List of analyzed listvenite cores and areas measured by XRFCL.

Hole Core-Section Interval	Top depth (m downhole)	Bottom depth (m downhole)	Z-axis (cm)		X-axis (cm)		Total number of spots
			min	max	min	max	
BT1B-12Z-1A, 84-89 cm	18.69	18.74	84.0	89.0	–3.0	3.0	143
BT1B-13Z-4A, 5-15 cm	23.82	23.92	5.0	15.0	–1.5	1.5	147
BT1B-14Z-2A, 0-64 cm	24.58	25.19	0.5	61.5	–3.0	3.0	1599
BT1B-16Z-3A, 7-40 cm	28.88	29.21	7.0	40.0	–3.0	3.0	871
BT1B-20Z-1A, 78-83 cm	39.98	40.03	6.5	10.5	–3.0	3.0	117
BT1B-28Z-1A, 49-70 cm	60.24	60.45	2.1	19.6	–2.5	2.5	396
BT1B-28Z-1A, 69-74 cm	60.44	60.49	8.3	12.3	–2.5	2.5	99
BT1B-32Z-2A, 70-85 cm	68.15	68.30	12.0	27.0	–3.0	3.0	403
BT1B-32Z-3A, 15-30 cm	68.57	68.72	15.0	30.0	–3.0	3.0	403
BT1B-32Z-3A, 57-65 cm	68.99	69.07	6.0	14.0	–3.0	3.0	221
BT1B-32Z-4A, 0-12 cm	69.27	69.38	0.0	12.0	–3.0	3.0	325
BT1B-47Z-4A, 41-50 cm	108.91	109.00	60.0	69.0	–1.5	1.5	133
BT1B-49Z-1A, 20-55 cm	111.55	111.90	20.0	55.0	–2.0	2.0	639
BT1B-49Z-2A, 6-34 cm	112.13	112.41	47.0	74.0	–2.0	2.0	513
BT1B-52Z-3A, 1-4 cm	119.65	119.68	4.5	9.0	–3.0	3.0	130
BT1B-52Z-3A, 39-46 cm	120.03	120.10	13.0	20.0	–3.0	3.0	195
BT1B-53Z-4A, 37-47 cm	124.08	124.18	60.0	70.0	–1.5	1.5	147
BT1B-60Z-1A, 12-17 cm	139.97	140.02	6.5	10.5	–3.0	3.0	117
BT1B-66Z-3A, 66-71 cm	160.60	160.65	6.0	10.0	–3.0	3.0	117
BT1B-73Z-2A, 16-22 cm	180.43	180.49	4.0	10.0	–2.25	2.25	130

Table S2. Parameters obtained from the multiple linear regression

	Constant		
SiO2	-5.16	±	0.10
MgO	-3.83	±	0.10
CaO	1.26	±	0.11
Intercept	3489.64	±	8.80

Reference

Nicolas, A., Boudier, F., Ildefonse, B., & Ball, E. (2000). Accretion of Oman and United Arab Emirates ophiolite–Discussion of a new structural map. *Marine Geophysical Researches, 21*(3-4), 147-180.